Thermochimica Acta 706 (2021) 179053

Contents lists available at ScienceDirect

Thermochimica Acta

journal homepage: www.elsevier.com/locate/tca

Experimental method to determine specific heat capacity and transition enthalpy at a first-order phase transition: Fundamentals and application to a Ni-Mn-In Heusler alloy

F.J. Romero *, M.C. Gallardo, J.-M. Martín-Olalla, J. del Cerro

Departamento de Física de la Materia Condensada, Facultad de Física, ICMSE-CSIC. Universidad de Sevilla, Avenida Reina Mercedes s/n ES41012 Sevilla, Spain

ARTICLE INFO

Keywords:
Specific heat capacity
Latent heat
Enthalpy
Phase transition
Heusler alloy

ABSTRACT

A new method that characterizes thermal properties during a first-order phase transition is described. The technique consists in exciting the sample by a series of constant frequency thermal pulses which one in every N pulses –N is a small number like four—being exceedingly large in amplitude. This pulse induces phase transformation which is inhibited during the following smaller pulses due to thermal hysteresis. That way the specific heat capacity for a given mixture of phases can be determined. The results obtained are independent of experimental parameters like the rate and the amplitude of the pulses, unlike what happens in other calorimetric techniques. The method also provides the enthalpy excess by analysing the energy balance between the dissipated heat and the heat flowing during each pulse of measurement.

The protocol is tested to analyse the phase transitions of a Heusler alloy $Ni_{50.53}Mn_{33.65}In_{15.82}$. The paramagnetic-ferromagnetic transition for the austenite phase is continuous and the specific heat capacity shows a lambda anomaly. The martensitic phase transition shows a first-order character and the specific heat capacity follows a step-like behaviour.

1. Introduction

The measure of thermal properties such as specific heat capacity, enthalpy and entropy is paramount in many topics of physics, chemistry or materials science [1] like the characterization of phase transitions. Thermal properties integrate every contribution to the free energy of the system and thus provide a unique information of the system.

First-order phase transitions are characterized by a few defining properties. They ideally happen at a given temperature. Energy exchange does not cause the sample to heat or cool (sensible heat), instead it causes phase transformation (latent heat) altering the molar fraction of coexisting phases [2]. Thermal properties like entropy and enthalpy excesses show a discontinuity while the specific heat capacity has a singularity at the transition point since the exchange of energy does not cause a change of temperature. An additional feature is the presence of thermal hysteresis between cooling and heating runs.

In real systems this sharp behaviour is usually smeared: temperature gradients, internal stresses, sample inhomogeneities, defects and the like make the transition to happen over an extended range of temperature. The latent heat spreads over that temperature interval and there is also a variation of the specific heat capacity since some fraction of the sample is modifying its temperature. As a result of all this, the measure of thermal properties during a first-order phase transition is always challenging.

Specific heat capacity c is a primordial property for the thermal characterization of a sample. By integrating the specific heat capacity over temperature, changes of enthalpy over a range of temperature are evaluated. Likewise by integrating c/T, changes of entropy are determined. In the simplest case specific heat capacity is measured by exciting the sample with a thermal pulse; the ratio of the pulse to the change of temperature evaluates the specific heat capacity as per its raw definition.

In first-order phase transitions the experimentalist must discriminate which portion of the heat pulse caused phase transformation (latent heat) and which portion, if any at all, caused a change of temperature (sensible heat). Both contribute to the total change of enthalpy over an extended range of temperature.

Specific heat capacity data obtained in presence of latent heat may not be reproducible because they could depend on the experimental setup including parameters like the amplitude of the heat pulses and the

* Corresponding author.
E-mail addresses: fjromero@us.es (F.J. Romero), mcgallar@us.es (M.C. Gallardo), olalla@us.es (J.-M. Martín-Olalla), delcerro@us.es (J. del Cerro).

https://doi.org/10.1016/j.tca.2021.179053
Received 19 February 2021; Received in revised form 16 September 2021; Accepted 21 September 2021
Available online 28 September 2021

temperature variation rate.

Adiabatic calorimetry is an excellent tool for measuring heat capacity data. However, an intrinsic inaccuracy in the values obtained in the vicinity of a first-order phase transition has been discussed [3]. During a first order phase transition the sample ceases to be a passive element whose temperature increases as energy is dissipated by the heater. Instead, the sample is able to absorb/release energy without increasing/decreasing its temperature. Therefore, the energy balance by which specific heat capacity is determined in adiabatic calorimetry is compromised.

Although high ac calorimetry [4] has a very good temperature resolution, it has been extensively used to study second-order phase transition because it measures heat capacity and it is unable to analyse total enthalpy [5]. On the contrary, differential scanning calorimetry and differential thermal analysis [1] are able to compute total enthalpy changes although the temperature resolution is not good as a consequence of the fast scan rates. However, it is hard to discriminate specific heat capacity contribution and latent heat contributions. Temperature modulated differential scanning calorimetry (TMDSC) combines ac calorimetry and DSC and the temperature ramp is modulated by an alternative component [6,7] to separate the reversing and the non-reversing contributions to the specific heat capacity.

It must be also noticed that the application of commercial heat-flow sensors (Peltier cells) has allowed to build new calorimeters especially suitable to determine the heat capacity and the magnetocaloric effect in first-order phase transitions. The design allows to miniaturize the assembly by using large figure of merit semiconductor thermopiles [8,9]. Microcalorimetry has also been used to study small distributed latent heats and to separate it from the specific heat capacity by using membrane-based microcalorimeters [10].

Relaxation calorimetry has been shown to be an excellent technique to determine heat capacities [11]. The growing availability of commercial, fully automated relaxation calorimetry (specifically the physical property measurement system PPMS from Quantum Design QD) has allowed to extend this type of calorimetry. The standard method, consisting in fitting the heating and cooling branches obtained when the temperature of the sample is modified by a heat pulse, is not appropriate for first-order phase transitions [12]. Different approaches have been done to study first-order phase transitions. The single pulse method consists in applying a temperature pulse large enough to wholly cross the phase transition [13]. For materials with transitions extended over dozens of degrees this method cannot be applied. A different method (successive heating pulses) has been described [14] where a series of short heating pulses (temperature increment lower than 2 K) is applied at equally spaced temperatures (typically 2 K) across the transition interval, preceded by a long-time stabilization before the power is applied. The key point is that there should not be overlap between the temperatures reached in two consecutive pulses.

We previously developed a method called Squared Modulated Differential Thermal Analysis (SMDTA) which is able to characterize continuous (second-order) and discontinuous (first-order) phase transitions [15,16] even in the neighbourhood of a tricritical point where the challenges grow because the specific heat capacity is expected to diverge. In this technique the specific heat capacity is measured by exciting the sample with a series of identical square thermal pulses superposed to a linear temperature ramp.

To allow a more precise study of first-order phase transitions a procedure was developed which consists in combining the results of two experiments on the same sample and under similar temperature variation rates. In the first experiment, the specific heat capacity was determined with aforementioned method. Then a second run recorded the fluxmeter signal under the same linear temperature ramp with no other external excitation, which is a high sensitive differential thermal analysis.

Later, we showed that the analysis of the data from the transient response of the fluxmeters during the specific heat capacity measurement (with the sample being excited by the series of thermal pulses) allowed to obtain a signal which is equivalent to the DTA trace of the second experiment [16]. Therefore, the second experiment became unnecessary. However, a challenge remained: discriminating the specific heat capacity and latent heat during a first order phase transition due to the influence of the latent heat on the transient response during the measurement.

This paper introduces an improvement of the SMDTA technique that allows the measurement of the heat capacity during a first-order phase transition. Unlike the original method, the new technique employs amplitude-modulated thermal pulses, with one in every N pulses being exceedingly large. We take advantage of the thermal hysteresis that follows the large thermal pulse and which inhibits subsequent phase transformations. The fundamental of the method could be applied to other types of calorimetry. For testing the method we choose a Heusler type alloy ($Ni_{50.53}Mn_{33.65}In_{15.82}$) which exhibits a second-order para-ferromagnetic phase transition followed by a first-order martensitic phase transition [17].

2. Experimental details

The experimental device has been described elsewhere [18]. The sample is sandwiched between two heat fluxmeters, rigid enough to support the sample and to apply, if necessary, a controlled uniaxial stress on the sample. The other end of each fluxmeter is in thermal contact with a calorimetric block. Two heaters, placed between the sample and the fluxmeters, allow us to supply heat pulses, whose effect is superposed to the temperature ramp. Heat pulses are able to achieve a temperature amplitude ranging from 0.01 K to 0.25 K. The signal of the fluxmeters is measured by a 2182 Keithley nanovoltmeter.

Sensors and heaters are placed in a cylindrical hole located axially in a cylindrical piece of bronze (10 kg) which serves as heat sink and constitutes the calorimeter block. The block temperature is determined from the resistance of a commercial platinum thermometer Leads and Northrup model 8164B measured by a Tinsley bridge model Ambassador. The block and two surrounding radiation shields are placed into a hermetic outer case under vacuum ($p = 1 \times 10^{-5}$Pa). The assembly, surrounded by a coiled tube, is placed in a Dewar jar filled with liquid refrigerant. The temperature of this bath is controlled by a close-cycle circulation of Thermal H5 provided by a thermostat (Julabo FP45).

Due to the high thermal inertial of the calorimetric block, the radiation shields and the high thermal capacity of the block, the temperature changes are some 10^{-3} K/h with temperature fluctuations of the calorimeter block smaller than 10^{-6} K.

The bridge can be used to measure to determine the temperature at the internal junction of the fluxmeters since the heaters are also calibrated as thermometers. It has been shown that the difference between the temperature of the block and the temperature of the internal junction of the fluxmeters is constant and about 0.001 K [19] due to the large thermal inertia of the device (10 kg in mass) and the operating temperature variation rates (10^{-5} Ks^{-1}).

The sample was prepared from the appropriate quantities of high-purity (99.9%) nickel, manganese, and indium from an unspecified

Table 1
Atomic composition from energy dispersive X-ray fluorescence and the corresponding electron per atom ratio, e/a.

At% Ni	50.53
At% Mn	33.65
At% In	15.82
e/a	7.883

Standard uncertainties u are u(At% Ni)= 0.09, u(At% Mn)=0.07, u(At% In)=0.08, and the combined standard uncertainty u_c(e/a)=0.005.

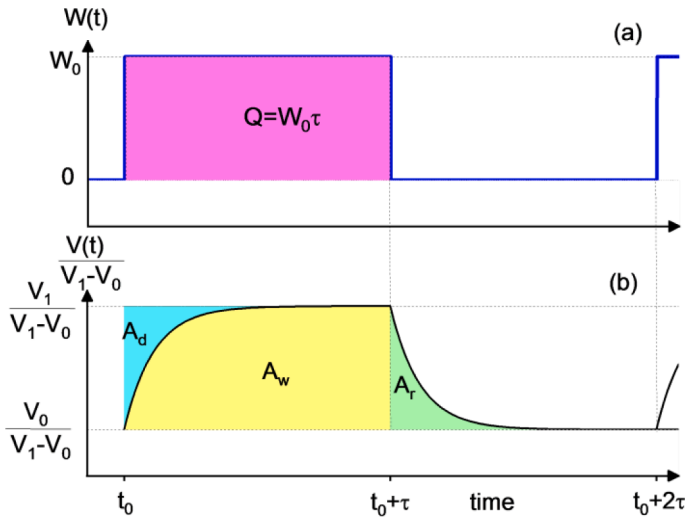

Fig. 1. (a) A square thermal pulse of amplitude W_0 and duration τ dissipating $Q = W_0\tau$ and (b) the response given by the fluxmeters scaled by the highest deviation V_1-V_0. The areas A_d, A_w and A_r (see Eqs. (1), (2) and (3)) are shaded.

commercial source. The metals were arc melted several times under an argon atmosphere, flipping the buttons each time. The buttons were then remelted and the alloy drop cast into a copper chill cast mould to ensure compositional homogeneity throughout the ingots. The crystals were grown in a resistance furnace from the as-cast ingots in an alumina Bridgman style crucible.

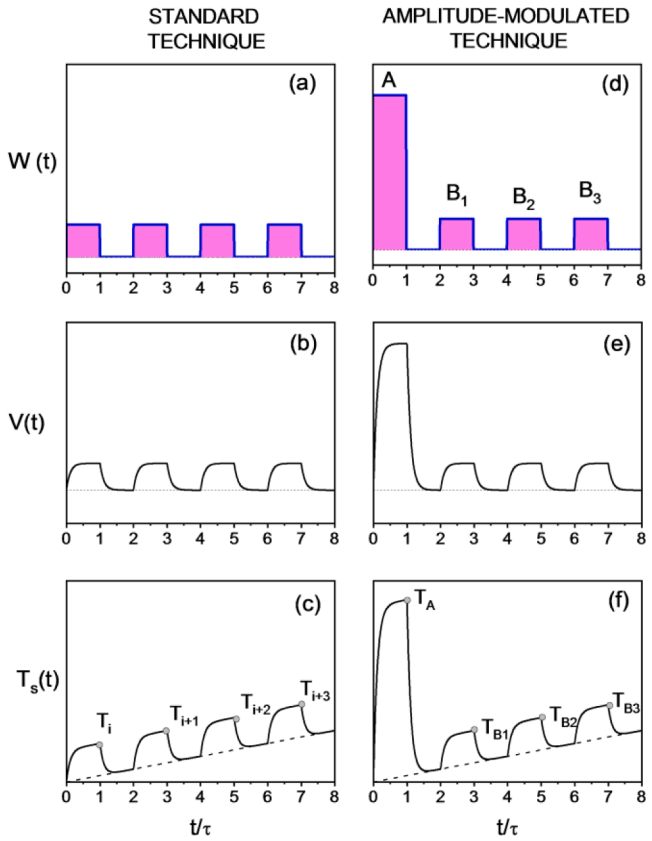

Fig. 2. On the left a schematic of the standard technique is represented: a train of square heat pulses with equal amplitude and period (a); the associated response given by the fluxmeters (b); and change of temperature in the sample if a stationary rate of temperature change is set on the calorimetric block (c). Note that $T_{i+1}>T_i$ always. On the right the schematic of the new protocol is represented: a train of square heat pulses of equal period but with modulated amplitude, the first out of four pulses is exceedingly large amplitude (d); the associated fluxmeter signal (e) and the expected change of temperature in the sample (f). Note that the parameters of the experiments are set so that $T_{Bi}<T_A$.

The sample was nearly octagonal with flat faces of area 90 mm^2 and 1.89 mm height. The mass of the sample was 1.5487 g. The average composition of the sample was determined by energy dispersive X-ray fluorescence measurements (spectrometer EDAX μFRXEAGLE III) at the Research, Technology and Innovation Centre (CITIUS, University of Sevilla, Spain). The resulting composition was $Ni_{50.53}Mn_{33.65}In_{15.82}$ (see Table 1). The electrons per atom e/a was calculated as the concentration-weighted average of the valence electrons, which are the electrons in the external s, p and partially occupied d orbitals of the constituents. The value of e/a for this sample is 7.883.

3. Method

The specific heat capacity of the sample is measured using the following procedure [20]. At time $t = t_0$ the heaters begin to supply a constant power W_0 for a time τ long enough to let the sample reach a steady state temperature distribution, characterized by a temperature difference ΔT_1 between the sample and the calorimetric block. At time $t_1=t_0+\tau$, the power W_0 is cut off and the sample relaxes to a new steady state temperature distribution at time $t_2=t_0+2\tau$. The electromotive force given by the fluxmeters $V(t)$ is measured during the described process. $V(t)$ is proportional to proportional to the heat flux $\phi(t)$ crossing the fluxmeters, $\phi(t) = V(t)/\alpha$, where α is the sensitivity of the fluxmeters, determined by calibration.

Fig. 1 shows an ideal square pulse (top) and the transient response $V(t)$ by the fluxmeters scaled by the highest deviation V_1-V_0. Three normalized areas can be defined:

$$A_w = \int_{t_0}^{t_0+\tau} \frac{V - V_0}{V_1 - V_0} dt \tag{1}$$

$$A_d = \tau - \int_{t_0}^{t_0+\tau} \frac{V - V_0}{V_1 - V_0} dt \tag{2}$$

$$A_r = \int_{t_0+\tau}^{t_0+2\tau} \frac{V - V_0}{V_1 - V_0} dt \tag{3}$$

The integral of the heat flux over the duration of one cycle amounts

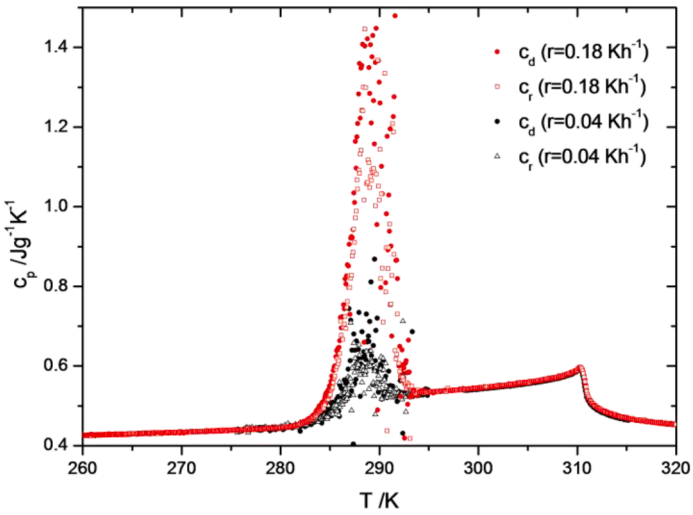

Fig. 3. Specific heat capacity data vs temperature in a $Ni_{50.53}Mn_{33.65}In_{15.82}$ sample. Specific heat capacity data for the dissipation branch (c_d) and for the relaxation branch (c_r) were obtained from Eq. (5) and 6 after a train of identical heat pulses excited the sample. Data in read stands for $r = 0.18$ K/h and $Q = 0.44$ J; data in black for $r = 0.04$ K/h and $Q = 0.11$ J. The reduction in r and Q decreases the peak height but increases the noise.

to the total energy supplied by the heaters $Q = W_0\,\tau$.

$$\int_{t_0}^{t_0+2\tau}(\phi-\phi_0)dt = \int_{t_0}^{t_0+2\tau}\frac{V-V_0}{\alpha}dt = \frac{(V_1-V_0)(A_w+A_r)}{\alpha} = W_0\tau = Q \qquad (4)$$

Two values of the specific heat capacity are obtained, c_d while the heaters are dissipating (dissipation branch) and c_r while there is no dissipation (relaxation branch) [15]:

$$mc_d = \frac{2}{\beta}\left(A_d - A_d^0\right) \qquad (5)$$

$$mc_r = \frac{2}{\beta}\left(A_r - A_r^0\right) \qquad (6)$$

where m is the mass of the sample, A_d^0 and A_r^0 are the areas when no sample is attached to the fluxmeters and β is the thermal resistance of the fluxmeters.

When no kinetic process is present, dissipation and relaxation branches are equivalent processes since the temperature of the sample changes equally in both branches and, consequently, the values of A_d and A_r coincide and, hence, c_d=c_r. The precision in the absolute value of the specific heat capacity was previously found to be in the range of 1% [21].

During a first order phase transition the relaxation branch and the dissipation branch may not be equivalent to each other as the latent heat is being absorbed or released. In this case, c_d and c_r could not coincide and they could even show non-regular behaviour due to the influence of the latent heat. This fact has been used to ascertain the temperature interval where a sharp first-order phase transition takes place [15].

Due to the large thermal inertia of the calorimetric block this protocol seldom operates in this equilibrium configuration. Instead it operates while the temperature of the calorimetric block is steadily varying at a low rate. Fig. 2 shows (panel a and b) a series of thermal pulses and responses; panel (c) shows the evolution of sample temperature with time when the temperature of the calorimetric block is steadily increasing.

When the temperature of the sample reaches a first-order phase transition the thermal pulse will trigger the phase transformation into the high temperature phase. Now energy is not stored as an increase of temperature (sensible heat) but as a structural transformation (latent heat). This will modify the response of the fluxmeters [16,22] and Eqs. (5) and (6) from which specific heat capacity is extracted do not hold.

Also in this case, the difference between the integral of the heat flux and Q is the enthalpy change exchanged in this cycle ΔH_i.

$$\Delta H_i = W_0\tau - \int_{t_0}^{t_0+2\tau}(\phi-\phi_0)dt = W_0\tau - \frac{1}{\alpha}\int_{t_0}^{t_0+2\tau}(V-V_0)dt \qquad (7)$$

Notice that in any of the cycles where the temperature of the sample is within the coexistence interval, the sample will be partially transformed to the high temperature phase since the temperature steadily increases with every cycle ($T_{i+1}>T_i$, see Fig. 2c). This fact will happen irrespective of the temperature variation range or the applied heat power.

The new method we present in this work is based in a train of N pulses of which the first one (A) is exceedingly large than the remaining pulses (B), see Fig. 2d. During a first-order phase transition pulse A will transform a fraction of the sample into the new high temperature phase but during the relaxation process thermal hysteresis will inhibit the backward transformation. Thereafter pulse B will not ideally induce new phase transformation since the temperature of sample does not exceed the maximum temperature reached during pulse A ($T_{Bi}<T_A$, see Fig. 2f). The transformation resumes only when the following pulse A is onset.

In this scenario the enthalpy excess can be determined from the energetic balance of the cycles. On the other hand reproducible specific heat capacity values can be obtained from Eq. (5) and (6) only for B-pulses. The normalized areas of pulses A are not related to specific heat capacity since phase transformation occurs in these cases and fluxmeter responses are distorted [16,22] as energy is structurally stored. These hypotheses will only be sound as long as the amplitude of pulse A, the amplitude of pulse B and the rate of change of temperature are appropriately set in the way that the temperature of the sample does not exceed maximum temperature reached on pulse A ($T_{Bi}<T_A$, see Fig. 2f). We recall that the phase transition takes place over an extended range of temperature due to internal stresses, inhomogeneities or defects, to name a few.

For each pulse, Eq. (7) is computed. For the first pulse it is expected that $\Delta H_i \neq 0$ if the transition is first-order. If the parameters are set appropriately for the following N-1 pulses or when no phase transition is occurring $Q_i = \tau W_i$ and the integral should match to each other within the experimental resolution.

The transition enthalpy will be calculated from $\Delta H_i = \sum_i \Delta H_i$ and the coexistence interval will be obtained by analysing the temperatures at which the condition $\Delta H_i \neq 0$ has been fulfilled.

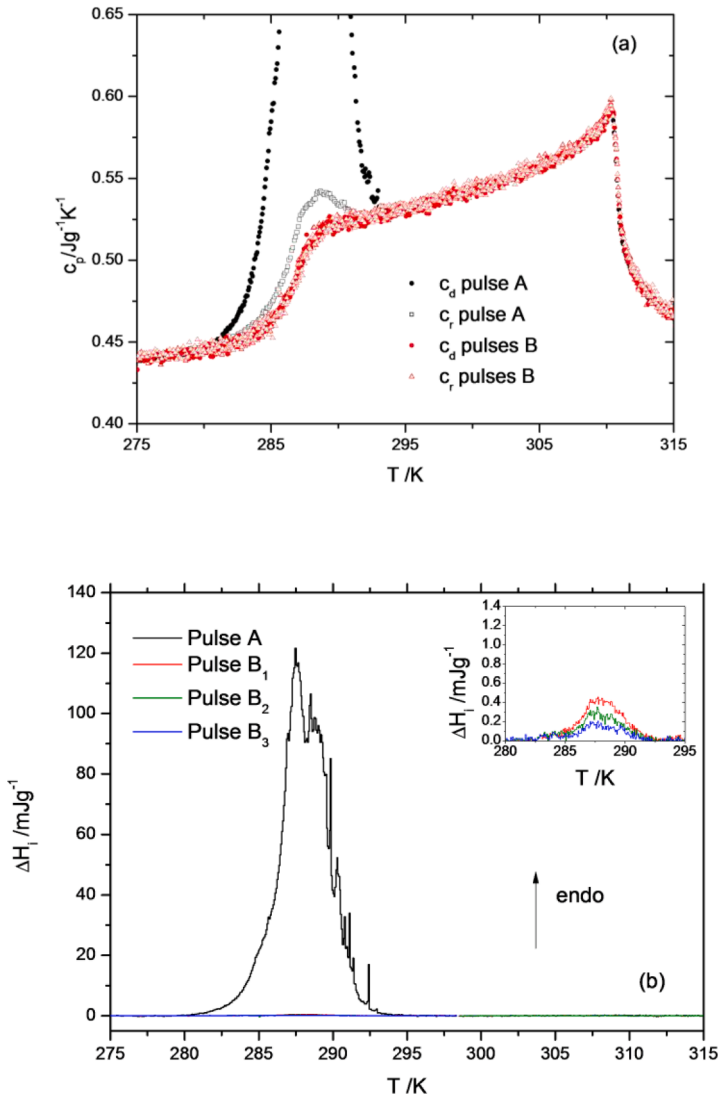

Fig. 4. (a) Specific heat capacity data vs temperature in a $Ni_{50.53}Mn_{33.65}In_{15.82}$ sample. Specific heat capacity data were obtained from a train of amplitude modulated heat pulses through Eq. (5) and 6, (b) ΔH_i vs temperature in the same run obtained from Eq. (7). The inset in panel (b) enlarges the coexistence interval for pulses B. The vertical axis in the inset spans for 1/100 of the span in the main plot.

4. Results and discussion

The new method was tested on a metamagnetic shape memory alloy Ni-Mn-In taking advantage of a series of phase transitions that happen in this alloy depending on the average electronic concentration e/a [23, 24]. When $7.86 < e/a < 7.90$, the alloy is in a ferromagnetic martensite phase at 100 K. On heating a paramagnetic martensite phase is formed at T_C^M and then a ferromagnetic austenite phase is formed at T_M (the temperature of the M transition). Further heating results in a magnetic phase transformation (FP transition) that brings the alloy to a paramagnetic austenite phase at the temperature T_C^A.

While T_C^A is weakly impacted by changes in the electronic concentration, T_M and T_C^M are strongly sensitive to changes in this parameter [24]. For our sample ($e/a = 7.883$), the M transition and the FP transition are expected to be close to each other and not far from room temperature. The M transition is first-order and the FP transition is second-order. Therefore, the experimental method can be tested in a single run on two different phase transitions without altering the experimental conditions.

In a first run, we recorded the specific heat capacity using the standard procedure [16,20] which consists of a series of identical square thermal pulses. We measured the time constant (78 s) and selected τ=720 s. The first run was performed under a temperature scanning rate $r = 0.18$ K/h (5.5×10^{-5} K/s) and the power dissipated ($W = 0.58$ mW, $Q = 0.42$ J) in the heaters was selected to produce a temperature increment $\Delta T = 0.035$ K at the end of the dissipation branch. Fig. 3 shows the specific heat capacity measured in the dissipation branch (red solid circles) and the specific heat capacity measured in the relaxation branch (red open squares) versus temperature from 260 K to 320 K.

At 310 K a lambda-like anomaly was found. We identify the temperature of the maximum of c_p, $T_C^A = 310.3$K, as the temperature of the FP transition. The standard uncertainty associated with T_C^A is $u(T_C^A) = 0.1$K after considering the window of temperature needed to measure the specific heat ($2r\tau$) and the increase of temperature ΔT associated with the dissipating power W. The value of T_C^A is in agreement with previous observations [23,25,26] and with the fact that T_C^A is weakly varying on e/a. [24]

Between 280 K and 294 K the specific heat capacity shows a large, broad excursion, in line with findings in Ni-Mn-In, Ni-Mn-In-Co and Ni-Mn-In-Sn alloys [17,23–29]. We identify this region as the martensite-austenite phase transition. We estimate the temperature of the martensite-austenite phase transition from the temperature at the

maximum of the specific heat as $T_M = 289.0$K . The standard uncertainty associated with T_M is $u(T_M) = 1.5$K. Notice that the latent heat, which extends over a wide temperature interval, makes the peak location of the martensite-austenite phase transition be less defined and eventually increases the uncertainty associated with T_M compared to $u(T_C^A)$.

The temperature location and the amplitude of the anomaly related to the martensitic phase transition in Ni-Mn-In alloys [17,23–27] changes abruptly with e/a in consonance with the phase diagram [24]: a change of 0.01 in e/a (1.4 per thousand) results in 12 K difference in T_M (4%). Therefore, an accurate determination of the sample composition, from which e/a is computed, is necessary. As an example, the composition of the sample in Ref. [23] $Ni_{50}Mn_{34}In_{16}$ is close to our composition ($Ni_{50.54}Mn_{33.65}In_{15.82}$) but e/a increases by 0.023 points from the value $e/a = 7.860$ in Ref [23] to our value $e/a = 7.883$ listed in Table 1. The change in T_M from 240 K [23] to our result 289 K is in line with the change in e/a. [24]

Except around the M transition c_d and c_r match to each other within experimental resolution. We have shown previously that a difference between c_d and c_r is an evidence of a first-order phase transition [15]. Martensitic phase transitions are known to show athermal behaviour, so that there is a distribution of transition temperatures and the latent heat spreads over a wide temperature interval. Scattering of c_d and c_r is likely to be due to the intermittent dynamic of the martensitic transformation which produces quasi-instantaneous heat flux peaks of different amplitudes and durations [30–34].

To shrink the fraction of sample that is transformed during each cycle we reduced the dissipated power ($W = 0.15$ mW, $Q = 0.11$ J, $\Delta T = 0.01$ K) as well as the temperature variation rate $r = 0.04$ K/h (1.1×10^{-5} K/s) in a second run. The results are also shown in Fig. 3 in black symbols. Data for the first and second run coincide over all the temperature interval except for the martensitic phase transition. There is no influence of the measuring parameters on the second order phase transition around 310 K. However, during the M transformation the second run produces an anomaly which is markedly lower and narrower than that observed in the first run. Interestingly c_d and c_r keep showing a noisy distribution, showing that some latent heat is disturbing the specific heat capacity measurement.

Therefore, experimental conditions impact the results. We stress the fact that this is happening even when the temperature scan rate is as low as 0.04 K/h (1.1×10^{-5} K/s) and the amplitude of the thermal pulse on the sample is as low as 0.01 K. The magnitude and the width of the peak depends on the experimental conditions that modify the kinetics of the transformation, even if the experimental device is not altered. Under different kinetics, the molar fraction of each phase evolves in a different way and the results for specific heat capacity data change. Therefore they cannot represent equilibrium values.

In a dynamic experiment, with temperature smoothly varying in time, latent heat and sensible heat are mixed up during a first-order phase transition which causes the measurement method to yield an effective, or generalized, specific heat capacity that blends both contributions. It provides valuable information about the phase transition and would allow the comparison of different samples if the experimental conditions do not change. Nevertheless, a distribution of peak heights can be traced for the martensite-austenite phase transition in Heusler alloys [17, 23–29]. In our set-up it is the right-hand side of Eq (5) and (6) that brings these effective values. Fig. 3 shows that our effective specific heat capacity actually depends on the experimental conditions and do not correspond to equilibrium values.

The new method was then tested. A train of $N = 4$ pulses was set with the first pulse (A) producing a temperature increment in the sample of 0.22 K ($W = 3.85$ mW, $Q = 2.80$ J) and the remaining three pulses (B) being 25 times smaller ($W = 0.15$ mW, $Q = 0.11$ J, $\Delta T = 0.01$ K). The scanning temperature rate for this experiment was 0.04 K/h.

Fig. 4a shows the results under these conditions. The new results markedly differ from the previous results only around the M transition, as we expected.

For A pulses the sample is markedly heated during the dissipation branch which, after some temperature is reached, makes the transformation begin. The associated enthalpy modifies the transient response by the fluxmeter and the stationary state cannot be reached in the prescribed time τ. Moreover the intermittent behaviour of the transformation characteristically induces heat peaks during the

Table 2
Specific heat capacity of $Ni_{50.53}Mn_{33.65}In_{15.82}$ as a function of the temperature at $p = 1.0 \times 10^{-5}$Pa. These data correspond to the values obtained from pulses B in the modified procedure. In the temperature interval between 280 K and 294 K the influence of the latent heat contribution has been removed.

T/K	c_p/Jg^{-1}K^{-1}	Phase
260.00	0.426	M
262.00	0.427	M
264.00	0.429	M
266.00	0.431	M
268.00	0.432	M
270.00	0.434	M
272.00	0.436	M
274.00	0.438	M
276.00	0.442	M
278.00	0.442	M
280.00	0.446	M
281.00	0.448	Mixed M+AF
282.00	0.449	Mixed M+AF
283.00	0.451	Mixed M+AF
284.00	0.458	Mixed M+AF
285.00	0.464	Mixed M+AF
286.00	0.477	Mixed M+AF
287.00	0.494	Mixed M+AF
288.00	0.513	Mixed M+AF
289.00	0.518	Mixed M+AF
290.00	0.524	Mixed M+AF
291.00	0.527	Mixed M+AF
292.00	0.523	Mixed M+AF
294.00	0.528	AF
296.00	0.533	AF
298.00	0.535	AF
300.00	0.542	AF
302.00	0.547	AF
304.00	0.556	AF
306.00	0.562	AF
308.00	0.570	AF
308.50	0.573	AF
309.00	0.578	AF
309.50	0.579	AF
310.00	0.591	AF
310.10	0.591	AF
310.20	0.591	AF
310.30	0.598	AP
310.40	0.592	AP
310.50	0.590	AP
310.60	0.581	AP
310.70	0.570	AP
310.80	0.556	AP
310.90	0.539	AP
311.00	0.527	AP
311.50	0.505	AP
312.00	0.495	AP
312.50	0.485	AP
313.00	0.480	AP
313.50	0.478	AP
314.00	0.471	AP
314.50	0.468	AP
316.00	0.466	AP
318.00	0.459	AP
320.00	0.454	AP

Standard uncertainties on temperature and pressure are $u(T) = 0.01$K and $u(p) = 5 \times 10^{-6}$Pa. The relative standard uncertainty of specific heat capacity is $u_r(c_p) = u(c_p)/c_p = 0.01$ for $T > 273$ K and $u_r(c_p) = u(c_p)/c_p = 0.02$ for $T < 273$ K. Phases: M martensitic phase, AF: ferromagnetic austenite, AP: paramagnetic austenite.

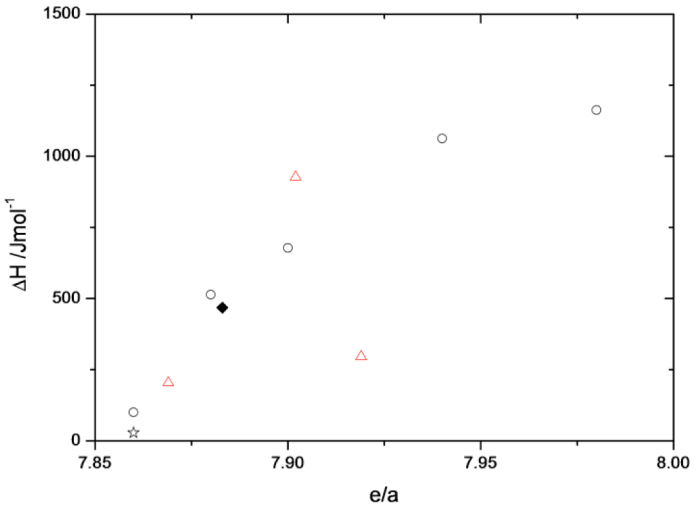

Fig. 5. The excess enthalpy for the M phase transition in different Ni-Mn-In alloys versus e/a: star [23], triangles [24], circles [35], diamond (this work).

dissipation branch. The thermal signature of these jerks extends to the relaxation branch). Globally speaking the dissipation and relaxation specific heat capacity c_d and c_r show a peak which is larger in amplitude and width for the dissipation branch.

Thermal hysteresis is expected to prevent the reversal transformation after the sample relaxes from pulse A. Notice that Ni-Mn-In compounds typically show hysteresis larger than 1 K in the M transformation. Ideally during a B pulse the dissipation branch should not be able to bring new transformations in the sample. Our experimental results fit to this hypothesis: the peak disappears for pulse B data while c_d and c_r match to each other within our experimental resolution. A selection of c_p data obtained following the new procedure is compiled in Table 2.

Fig. 4b shows ΔH_i (see Eq. (7)) versus temperature. For the FP phase transition, ΔH_i is zero for all the pulses, irrespective of their amplitude. This is the signature of a second order phase transition.

For the M transition, ΔH_i is markedly different from zero for A pulses. For B pulses, ΔH_i is about 0.4% of ΔH_i for A pulses (see the inset in panel (b)). The magnitude of the anomaly decreases for pulses B_2 and B_3. It indicates that although there is still a remnant phase transition taking place, the involved fraction of sample is much smaller.

Although the sensitivity of the system allows to measure such small enthalpy changes during B pulses, specific heat capacity data obtained for pulse B are less affected by the latent heat. While for A pulses $m\Delta H_i$ is 9% of Q at most, for B pulse it only amounts to 0.4% of Q at most, which is unable to exclude a null c_d-c_r within our experimental resolution.

The anomaly for c_p then looks like step-like transition in agreement with results obtained in a sample of the same family [25]. In this reference a peak was superimposed to the step anomaly. The peak is missed in our data after our technique dramatically reduces the impact of the latent heat in the measurement. The difference between the specific heat capacity for both phases could be related to the different magnetic character of both phases. Measurements of the magnetization would be necessary to ascertain the origin of the difference but this study is beyond the scope of this paper.

The enthalpy jump associated to the M transition is obtained by adding up ΔH_i for each cycle from 280 K to 295 K, where ΔH_i is non-zero. This yields $\Delta H = 7.06$ J/g or 468 J/mol, where the combined standard uncertainty associated with ΔH is $u(\Delta H) = 0.03\ \mathrm{Jg^{-1}} = 2\ \mathrm{Jmol^{-1}}$. This result combined with the electronic concentration e/a of the sample is in line with previously reported values for $Ni_{0.50}Mn_{0.50-x}In_x$. [23,24,35] (see Fig. 5). The fact that e/a for the sample in Ref. [23] is smaller than our value justifies the lower value for the enthalpy jump in that sample.

5. Conclusions

A new technique able to improve the discrimination of transition enthalpy (energy stored structurally) from specific heat capacity (energy stored kinetically) in first-order structural phase transitions has been designed and successfully tested on a sample of $Ni_{50.53}Mn_{33.65}In_{15.82}$.

The technique uses amplitude-modulated heat pulses during heating scans. The amplitude of one in every four pulses is exceedingly large ($\Delta T \sim 0.2$ K) so as to induce phase transformation which stores energy structurally and gives rise to transition enthalpy. In the remaining pulses the amplitude is decreased by a factor 25 so that phase transformation is almost inhibited due to hysteresis and the specific heat capacity for the given molar fraction of phases can be determined.

For the $Ni_{50.53}Mn_{33.65}In_{15.82}$ phase transitions, the results show that the ferromagnetic-paramagnetic transition is continuous while the martensitic phase transition is discontinuous. In the latter, the standard procedure gives an effective heat capacity which includes the contributions from the specific heat capacity and the latent heat. The effective heat capacity gives valuable calorimetric information but depends on the temperature variation rate and the heat dissipated during the measurement and cannot be easily related to equilibrium values.

The new protocol represents a progress in the SMDTA technique when it is applied to the study of first-order phase transition with a large thermal hysteresis like in shape memory alloys like the sample studied in this work. The extended thermal hysteresis allows the inhibition of the phase transformation during the smaller pulses, resulting in a better characterization of the transition, since the measured specific heat capacity data are closer to the equilibrium values. This specific heat capacity smoothly changes during the coexistence interval from the austenite value to the martensite value, in contrast with the peak which would is observed under the idea of an effective specific heat capacity that mixes both contributions. The latent heat is also determined from the energetic balance of each pulse.

Should the thermal hysteresis of a phase transition be smaller, a reduction in the temperature amplitude of the pulses and in the rate of temperature change would be mandatory to accomplish the condition $T_a > T_b$. In the case of a first-order phase transition with little thermal hysteresis, the standard protocol could be used.

The large heat capacity of the addenda in our device (which is attributed mainly to the fluxmeters) requires samples above 200 mg and sets a constant time of several tens of seconds. We are now working in a new device based in the miniaturization of the assembly and the thermopiles which would allow to study smaller samples and to reduce the time necessary to perform the measurements.

The amplitude modulated design of heat pulses could be also applied

to other calorimetric techniques which take advantage of heat pulses to measure specific heat capacity.

A bold challenge is to adapt the amplitude modulation to cooling scans. This would require to replace the heaters by a Peltier or a thermomagnetic device because in cooling scans phase transformation requires further active cooling.

CRediT authorship contribution statement

F.J. Romero: Conceptualization, Methodology, Investigation, Writing – original draft, Writing – review & editing, Visualization. **M.C. Gallardo:** Writing – review & editing, Project administration. **J.-M. Martín-Olalla:** Writing – review & editing, Visualization. **J. del Cerro:** Writing – original draft, Writing – review & editing.

Declaration of Competing Interest

The authors declare that they have no known competing financial interests or personal relationships that could have appeared to influence the work reported in this paper.

Acknowledgments

The authors wish to thank Prof. A. Planes (Universitat de Barcelona) for supplying the sample and Dr. R. Cano (Universidad de Sevilla) for his help in cutting the sample.

Supplementary materials

Supplementary material associated with this article can be found, in the online version, at doi:10.1016/j.tca.2021.179053.

References

[1] B. Wunderlich. Thermal Analysis, Academic Press, 1990, https://doi.org/10.1016/B978-0-12-765605-2.50005-4 https://doi.org/10.1016/B978-0-12-765605-2.50005-4.
[2] M.W. Zemansky, Heat and thermodynamics; an Intermediate Textbook, 5th edition, New York, McGraw-Hill, 1968 n.d. https://search.library.wisc.edu/catalog/999473407602121.
[3] V.K. Pecharsky, K.A. Gschneidner, Heat capacity near first order phase transitions and the magnetocaloric effect: an analysis of the errors, and a case study of Gd5(Si2Ge2) and Dy, J. Appl. Phys. 86 (1999) 6315–6321, https://doi.org/10.1063/1.371734.
[4] P.F. Sullivan, G. Seidel, Steady-State, ac-Temperature Calorimetry, Phys. Rev. 173 (1968) 679–685, https://doi.org/10.1103/PhysRev.173.679.
[5] C.W. Garland, High-resolution ac calorimetry and critical behavior at phase transitions, Thermochim. Acta. 88 (1985) 127–142, https://doi.org/10.1016/0040-6031(85)85420-4, https://doi.org/.
[6] B. Wunderlich, Modeling the heat flow and heat capacity of modulated differential scanning calorimetry, J. Therm. Anal. 48 (1997) 207–224, https://doi.org/10.1007/BF01979265.
[7] M. Reading, D. Elliott, V.L. Hill, A new approach to the calorimetric investigation of physical and chemical transitions, J. Therm. Anal. 40 (1993) 949–955, https://doi.org/10.1007/BF02546854.
[8] T. Plackowski, Y. Wang, A. Junod, Specific heat and magnetocaloric effect measurements using commercial heat-flow sensors, Rev. Sci. Instrum. 73 (2002) 2755–2765, https://doi.org/10.1063/1.1480452.
[9] V. Basso, C.P. Sasso, M. Küpferling, A Peltier cells differential calorimeter with kinetic correction for the measurement of cp(H,T) and Δs(H,T) of magnetocaloric materials, Rev. Sci. Instrum. 81 (2010), 113904, https://doi.org/10.1063/1.3499253.
[10] K. Morrison, M. Bratko, J. Turcaud, A. Berenov, A.D. Caplin, L.F. Cohen, A calorimetric method to detect a weak or distributed latent heat contribution at first order magnetic transitions, Rev. Sci. Instrum. 83 (2012), 33901, https://doi.org/10.1063/1.3690381.
[11] R. Bachmann, F.J. DiSalvo, T.H. Geballe, R.L. Greene, R.E. Howard, C.N. King, H. C. Kirsch, K.N. Lee, R.E. Schwall, H.-U. Thomas, R.B. Zubeck, Heat Capacity Measurements on Small Samples at Low Temperatures, Rev. Sci. Instrum. 43 (1972) 205–214, https://doi.org/10.1063/1.1685596.
[12] H. Suzuki, A. Inaba, C. Meingast, Accurate heat capacity data at phase transitions from relaxation calorimetry, Cryogenics (Guildf) 50 (2010) 693–699, https://doi.org/10.1016/j.cryogenics.2010.07.003, https://doi.org/.
[13] V. Hardy, Y. Bréard, C. Martin, Derivation of the heat capacity anomaly at a first-order transition by using a semi-adiabatic relaxation technique, J. Phys. Condens. Matter. 21 (2009) 75403, https://doi.org/10.1088/0953-8984/21/7/075403.
[14] F. Guillou, P. Courtois, L. Porcar, P. Plaindoux, D. Bourgault, V. Hardy, Calorimetric investigation of the magnetocaloric effect in Ni45Co5Mn37.5In12.5, J. Phys. D. Appl. Phys. 45 (2012), 255001, https://doi.org/10.1088/0022-3727/45/25/255001.
[15] J. del Cerro, J.M. Martín-Olalla, F.J. Romero, Square modulated differential thermal analysis, Thermochim. Acta. 401 (2003) 149–158, https://doi.org/10.1016/S0040-6031(02)00545-2.
[16] J. Del Cerro, J. Manchado, F.J. Romero, M.C. Gallardo, Square-modulated differential thermal analysis: measuring method, Meas. Sci. Technol. 23 (2012) 35003, https://doi.org/10.1088/0957-0233/23/3/035003.
[17] V.K. Sharma, M.K. Chattopadhyay, R. Kumar, T. Ganguli, P. Tiwari, S.B. Roy, Magnetocaloric effect in Heusler alloys Ni50Mn 34In16 and Ni50Mn34Sn16, J. Phys. Condens. Matter. 19 (2007), 496207, https://doi.org/10.1088/0953-8984/19/49/496207.
[18] M.C. Gallardo, J. Jiménez, J. del Cerro, Experimental device for measuring the influence of a uniaxial stress on specific heat: application to the strontium titanate ferroelastic crystal, Rev. Sci. Instrum. 66 (1995) 5288–5291, https://doi.org/10.1063/1.1146100.
[19] M.C. Gallardo, J. Jimenez, M. Koralewski, J. del Cerro, First order transitions by conduction calorimetry: application to deuterated potassium dihydrogen phosphate ferroelastic crystal under uniaxial pressure, J. Appl. Phys. 81 (1997) 2584–2589, https://doi.org/10.1063/1.363922.
[20] J. del Cerro, New measurement method of thermal properties by means of flux calorimetry, J. Phys. E. 20 (1987) 609–611, https://doi.org/10.1088/0022-3735/20/6/005.
[21] J. del Cerro, S. Ramos, J.M. Sanchez-Laulhe, Flux calorimeter for measuring thermophysical properties of solids: study of TGS, J. Phys. E. 20 (1987) 612–614, https://doi.org/10.1088/0022-3735/20/6/006.
[22] F.J. Romero, M.C. Gallardo, A. Czarnecka, M. Koralewski, J. Del Cerro, Thermal and kinetic study of the ferroelectric phase transition in deuterated triglycine selenate, J. Therm. Anal. Calorim. 87 (2007) 355–361, https://doi.org/10.1007/s10973-005-7444-7.
[23] X. Moya, L. Mañosa, A. Planes, S. Aksoy, M. Acet, E.F. Wassermann, T. Krenke, Cooling and heating by adiabatic magnetization in the Ni50 Mn34 In16 magnetic shape-memory alloy, Phys. Rev. B - Condens. Matter Mater. Phys. 75 (2007), 184412, https://doi.org/10.1103/PhysRevB.75.184412.
[24] T. Krenke, M. Acet, E.F. Wassermann, X. Moya, L. Mañosa, A. Planes, Ferromagnetism in the austenitic and martensitic states of Ni-Mn-In alloys, Phys. Rev. B - Condens. Matter Mater. Phys. 73 (2006), 174413, https://doi.org/10.1103/PhysRevB.73.174413.
[25] A.B. Batdalov, A.M. Aliev, L.N. Khanov, V.D. Buchel'nikov, V.V. Sokolovskii, V. V. Koledov, V.G. Shavrov, A.V. Mashirov, E.T. Dil'mieva, Magnetic, thermal, and electrical properties of an Ni45.37Mn40.91In13.72 Heusler alloy, J. Exp. Theor. Phys. 122 (2016) 874–882, https://doi.org/10.1134/S1063776116040129.
[26] M.K. Chattopadhyay, M.A. Manekar, V.K. Sharma, P. Arora, P. Tiwari, M.K. Tiwari, S.B. Roy, Contrasting magnetic behavior of Ni50Mn35In 15and Ni50Mn34.5In15.5 alloys, J. Appl. Phys. (2010) 108, https://doi.org/10.1063/1.3478774.
[27] J.-H.H. Chen, N.M. Bruno, I. Karaman, Y. Huang, J. Li, J.H. Ross, Calorimetric and magnetic study for Ni50Mn36In14 and relative cooling power in paramagnetic inverse magnetocaloric systems, J. Appl. Phys. 116 (2014), 203901, https://doi.org/10.1063/1.4902527.
[28] A.N. Vasiliev, O. Heczko, O.S. Volkova, T.N. Vasilchikova, T.N. Voloshok, K. V. Klimov, W. Ito, R. Kainuma, K. Ishida, K. Oikawa, S. Fähler, On the electronic origin of the inverse magnetocaloric effect in Ni-Co-Mn-In Heusler alloys, J. Phys. D. Appl. Phys. (2010) 43, https://doi.org/10.1088/0022-3727/43/5/055004.
[29] S.M. Podgornykh, E.G. Gerasimov, N.V. Mushnikov, T. Kanomata, Heat capacity of the Ni50Mn37(In0.2Sn 0.8)13 alloy, J. Phys. Conf. Ser. 266 (2011), 012004, https://doi.org/10.1088/1742-6596/266/1/012004, 0–5.
[30] M.C. Gallardo, J. Manchado, F.J. Romero, J. Del Cerro, E.K.H. Salje, A. Planes, E. Vives, R. Romero, M. Stipcich, Avalanche criticality in the martensitic transition of Cu67.64 Zn16.71 Al15.65 shape-memory alloy: a calorimetric and acoustic emission study, Phys. Rev. B - Condens. Matter Mater. Phys. 81 (2010), 174102, https://doi.org/10.1103/PhysRevB.81.174102.
[31] F.J. Romero, J. Manchado, J.M. Martn-Olalla, M.C. Gallardo, E.K.H. Salje, Dynamic heat flux experiments in Cu67.64Zn16.71Al15.65: separating the time scales of fast and ultra-slow kinetic processes in martensitic transformations, Appl. Phys. Lett. 99 (2011) 11906, https://doi.org/10.1063/1.3609239.
[32] J. Baró, J.-.M. Martín-Olalla, F.J. Romero, M.C. Gallardo, E.K.H. Salje, E. Vives, A. Planes, Avalanche correlations in the martensitic transition of a Cu–Zn–Al shape memory alloy: analysis of acoustic emission and calorimetry, J. Phys. Condens. Matter. 26 (2014), 125401, https://doi.org/10.1088/0953-8984/26/12/125401.
[33] F.J. Romero, J.M. Martín-Olalla, M.C. Gallardo, D. Soto-Parra, E.K.H. Salje, E. Vives, A. Planes, Scale-invariant avalanche dynamics in the temperature-driven martensitic transition of a Cu-Al-Be single crystal, Phys. Rev. B. 99 (2019), 224101, https://doi.org/10.1103/PhysRevB.99.224101.
[34] E. Vives, J. Baró, M.C. Gallardo, J.M. Martín-Olalla, F.J. Romero, S.L. Driver, M. A. Carpenter, E.K.H. Salje, M. Stipcich, R. Romero, A. Planes, Avalanche criticalities and elastic and calorimetric anomalies of the transition from cubic Cu-Al-Ni to a mixture of 18R and 2H structures, Phys. Rev. B. 94 (2016), 024102, https://doi.org/10.1103/PhysRevB.94.024102.
[35] W. Ito, Y. Imano, R. Kainuma, Y. Sutou, K. Oikawa, K. Ishida, Martensitic and Magnetic Transformation Behaviors in Heusler-Type NiMnIn and NiCoMnIn Metamagnetic Shape Memory Alloys, Metall. Mater. Trans. A. 38 (2007) 759–766, https://doi.org/10.1007/s11661-007-9094-9.